Controlling the strong field fragmentation of $ClCHO^+$ using two laser pulses –an ab initio molecular dynamics simulation

Xuetao Shi, and H. Bernhard Schlegel*

For a single, intense 7 μm linearly polarized laser pulse, we found that the branching ratio for the fragmentation of $ClCHO^+$ → Cl + HCO^+, H + $ClCO^+$, HCl^++CO depended strongly on the orientation of the molecule (*J. Phys. Chem. Lett.* **2012**, *3* 2541). The present study explores the possibility of controlling the branching ratio for fragmentation by using two independent pulses with different frequencies, alignment and delay. Born-Oppenheimer molecular dynamics simulations in the laser field were carried out with the B3LYP/6-311G(d,p) level of theory using combinations of 3.5, 7 and 10.5 μm sine squared pulses with field strengths of 0.03 au (peak intensity of 3.15×10^{13} W/cm^2) and lengths of 560 fs. A 3.5 μm pulse aligned with the C-H bond and a 10.5 μm pulse perpendicular to the C-H bond produced a larger branching ratio for HCl^++CO than a comparable single 7 μm pulse. When the 10.5 μm pulse was delayed by one quarter of the pulse envelope, the branching ratio for the high energy product, (HCl^++CO 73%) was a factor of three larger than the low energy product (Cl + HCO^+, 25%). By contrast, when the 3.5 μm pulse was delayed by one quarter of the pulse envelope, the branching ratio was reversed (HCl^++CO 38%; Cl + HCO^+, 60%). Continuous wavelet analysis was used to follow the interaction of the laser with the various vibrational modes as a function of time. © 2018 Wiley Periodicals, Inc.

DOI:10.1002/jcc.25576

Introduction

Chemists have been wanting to perform mode-selective chemistry since the development of the laser in the 1970s.[1–8] However, because of rapid intramolecular vibrational energy redistribution (IVR) in polyatomic molecules, this goal has remained elusive. In principle, mode-selectivity can be achieved if specific vibrational modes are excited efficiently and the reaction proceeds faster than IVR.[1–8] In a previous study[9], we used Born-Oppenheimer molecular dynamics (BOMD) to demonstrate that selective reaction acceleration can be obtained for oriented $ClCHO^+$ molecule with an ultra-short, intense, linearly polarized mid-IR laser pulse. In related studies, we have used BOMD simulations with similar mid-IR pulses to accelerate selective bond dissociation and to promote hydrogen migration in oriented molecules. [10–15]

There are three low energy channels for the dissociation of $ClCHO^+$. At the B3LYP/6-311G(d,p) level of theory the dissociation energies are:

$$\begin{aligned} ClCHO^+ + h\nu &\rightarrow Cl + HCO^+ \quad 7.0\,kcal/mol \\ &\rightarrow H + ClCO^+ \quad 30.2\,kcal/mol \\ &\rightarrow HCl^+ + CO \quad 30.9\,kcal/mol \end{aligned}$$

The calculated difference between the HCl^+ + CO and Cl + HCO^+ channels compares favorably with the experimental enthalpy difference of 19.2 kcal/mol.

Since the Cl dissociation channel is significantly lower in energy than the other two dissociation channels, classical trajectory calculations on the ground state Born-Oppenheimer potential energy surface showed that when the initial kinetic energy is distributed statistically, Cl dissociation channel is dominant.[9] However, an intense, 4 cycle 7 μm pulse perpendicular to the C–H bond direction enhances the higher energy HCl^+ dissociation channel. This reaction involves C-H and C-Cl bond breaking and H-Cl bond formation. It may be possible to promote these modes by separate, lower intensity pulses with different wavelengths and orientations. In the present study, we explore the possibility of facilitating this reaction using two independently selected laser pulses. For the sake of simplicity, the two laser pulses are restricted to be linearly polarized and of equal total duration, but the pulses can have different wavelengths, polarization orientations and relative timings. To get a better description of the interaction between the laser pulses and the molecule, we use a Continuous Wavelet Transformation (CWT)[16–18] of the trajectories to obtain information about the energy in various vibrational modes as a function of time during and after the laser pulse.

Methods

The simulations of dissociation were carried out by classical trajectory calculations on the ground state Born-Oppenheimer

[a] *X. Shi, H. B. Schlegel*
Department of Chemistry, Wayne State University, Detroit, Michigan, 48202, US
E-mail: hbs@chem.wayne.edu
Contract Grant sponsor: Division of Chemistry; Contract Grant number: CHE1464450; Contract Grant sponsor: National Science Foundation, Division of Chemistry; Contract Grant number: CHE1464450

surface for aligned formyl chloride cations in the time varying electric field of the laser pulses. As in our previous studies,[9–15] the B3LYP/6-311G(d,p) level of theory was chosen as a suitable compromise between accuracy of the potential energy surface and efficiency in the trajectory calculations. Molecular dynamics calculations were carried out with the development version of the Gaussian series of programs[19] and the PCvelV integrator[20] with a step size of 0.25 fs and Hessian updating[21,22] for 20 steps before recalculation of the Hessian. The starting structures had zero point energy but no rotational energy. Zero-point vibrational energy was added using orthant sampling of the momentum[23]. The polarization directions of the laser pulses are with respect to the initial orientation of the molecule; the molecule is free to rotate during the trajectory. Trajectories were integrated for a total of 1200 fs; 200 trajectories were calculated for each pulse sequence. A few trajectories gained large amounts of vibrational energy due to unphysically large charge oscillations within a single laser cycle. These were discarded as artifacts of the Born-Oppenheimer approximation. Based on previous experience with BOMD trajectories, most of these artifacts occur during C-H dissociation when a hydrogen atom is very far away (>10 Å) from the rest of the molecule while still in the oscillating laser field.

Trajectories were classified into specific channels (Cl + HCO^+, H + $ClCO^+$, HCl^+ + CO, no reaction) based on bond lengths. Vibrational energy transfer from the laser field was analyzed by performing Continuous Wavelet Transformation (CWT) on the vector components of the mass-weighted velocities of the individual atoms and the power spectra are summed over all of the trajectories in a given channel. The analysis was carried out with CWT implemented in a Python package.[24] CWT uses the following formula:

$$w(u,s)=\frac{1}{\sqrt{s}}\int_{-\infty}^{\infty}X(t)\psi^{*}\left(\frac{t-u}{s}\right)dt, \qquad (1)$$

where u, s are the translation and scaling parameters, $w(u, s)$ is the CWT of signal function $X(t)$, which in turns gives the power spectrum, $P(u, s) = w^{*}(u, s)w(u, s)$. $\psi\left(\frac{t-u}{s}\right)$ is a series of functions that parametrically depend on time-domain parameter u and frequency-domain parameter s (scaling parameter is the frequency inversed), generated from a mother wavelet function. In the present study, such mother wavelet function is the Gabor wavelet function,

$$\psi_{\omega}^{*}\left(\frac{t-u}{s}\right)=\frac{1}{\sqrt[4]{\pi}}e^{i\omega\left(\frac{t-u}{s}\right)}e^{-\frac{\left(\frac{t-u}{s}\right)^{2}}{2}}\ \text{with}\ \omega=6. \qquad (2)$$

Results and Discussion

Structure, frequencies and laser pulse parameters

The structure of formyl chloride cation is shown in Figure 1 and the vibrational frequencies of $ClCHO^+$ and its dissociation fragments are listed in Table 1. To induce dissociation, the laser pulses were selected to have wavelengths of 3.5, 7, 10.5 and 14 μm to cover the range of vibrations in $ClCHO^+$. While a single wavelength may be effective in causing H or Cl dissociation, two different wavelengths may be required to promote the rearrangement needed for HCl^+ dissociation. The two independent, linear polarized pulses were chosen to have a sine squared envelope, $\sin(\omega t/n)^2 \sin(\omega t)$, with a maximum field strength of 0.03 au (corresponding to a peak intensity of 3.15×10^{13} W/cm^2). Number of cycles for each wavelength (16 for 10.5 μm, 24 for 7 μm, 48 for 3.5 μm) was chosen to keep the total pulse duration the same (560 fs). For a two-pulse sequence, simulations were also carried out with the second pulse delayed by one quarter and one half of the pulse width (140 fs and 280 fs, respectively). Figure 2 shows a 3.5 μm pulse and a 10.5 μm pulse delayed by one quarter of the pulse width.

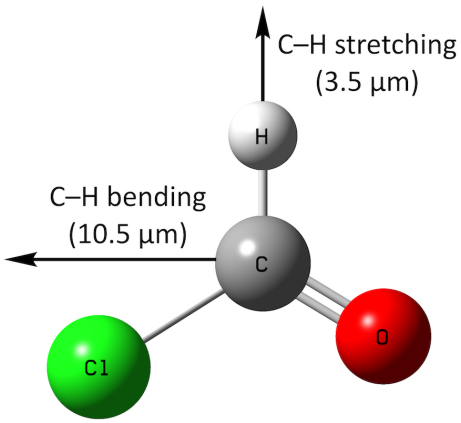

Figure 1. $ClCHO^+$ geometry and laser polarization directions. [Color figure can be viewed at wileyonlinelibrary.com]

The intensities and polarization directions of the vibrational modes of $ClCHO^+$ are shown in Figure 3. Also shown are some of the laser pulses and their spectral widths. Wavelengths of 3.5, 7, 10.5 and 14 μm (correspond to 2857, 1428, 952 and 714 cm^{-1} respectively), should interact with C–H stretching (2983 cm^{-1}), C–O stretching (1507 cm^{-1}), Cl–C–H bending (1174 cm^{-1}) and C-Cl stretching (731 cm^{-1}), respectively. The polarization direction of each laser pulse was aligned with the vibrational mode that it was chosen to promote (see Figure 1).

Table 1. Vibrational modes calculated at the B3LYP/6-311G(d,p) level for $ClCHO^+$ and its dissociation fragments.

species	mode	frequency (cm^{-1})	wavelength (μm)
$ClCHO^+$	Cl–C–O bend	233	42.99
	C–Cl stretch	732	13.67
	out-of-plane bend	908	11.02
	C–H bend	1174	8.52
	C–O stretch	1507	6.64
	C–H stretch	2983	3.35
H + $ClCO^+$	Cl–C–O bend	450	22.20
	C–Cl stretch	863	11.59
	C–O stretch	2376	4.21
Cl + HCO^+	C–H bend	865	11.56
	C–O stretch	2270	4.41
	C–H stretch	3229	3.10
CO + HCl^+	C–O stretch	2220	4.50
	H–Cl stretch	2635	3.79

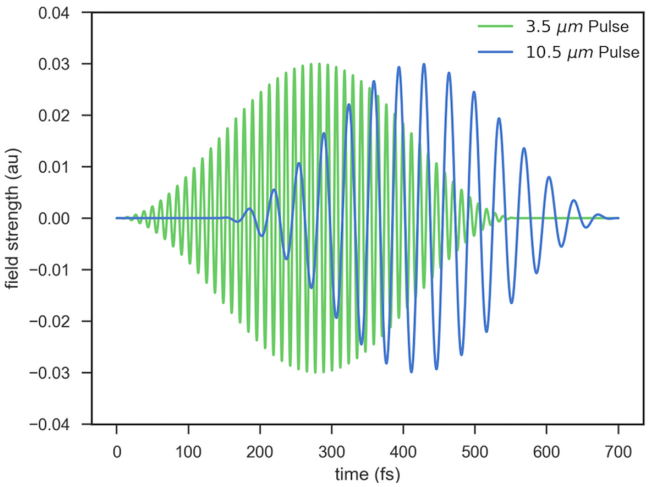

Figure 2. Electric field of a 3.5 μm pulse and a 10.5 μm pulse delayed by one quarter of the pulse width. [Color figure can be viewed at wileyonlinelibrary.com]

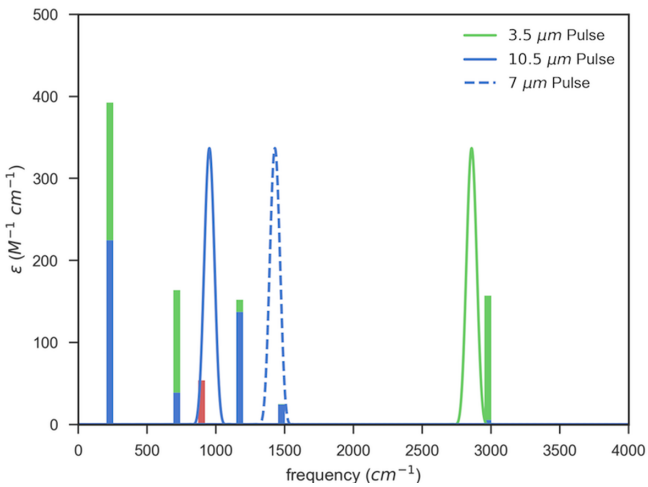

Figure 3. Infrared spectrum of $ClCHO^+$ showing the intensities and polarization directions of the various vibrational modes (green – along the C-H bond, blue – perpendicular to the C-H bond and in the plane, red – perpendicular to the plane). The line shapes of the 3.5, 7 and 10.5 μm pulses and their polarization directions are shown using the same color scheme. [Color figure can be viewed at wileyonlinelibrary.com]

Molecular dynamics in the laser field

The results of molecular dynamics simulations of the dissociation $ClCHO^+$ with two laser pulses are listed in Table 2. In earlier work,[9] we found that a single short, intense 7 μm laser pulse (90 fs, 0.09 au) perpendicular to the C–H bond successfully promoted the high energy channel for $ClCHO^+$ dissociating to HCl^+ + CO. Hence this wavelength and orientation can serve as reference for the various two pulse sequences in the present study. Two 7 μm pulses with field strength of 0.03 au with no delay are equal to a single 7 μm pulse with a field strength of 0.06 au. This pulse is not as strong as in the previous study and produced mainly Cl dissociation and only a few higher energy H and HCl^+ dissociations (2.3% and 19.0%, Table 2). Dissociation of Cl can be enhanced by aligning a 14 μm pulse with the C-Cl bond and a 7 μm pulse with the C=O bond. A 3.5 μm pulse along the C–H stretching direction combined with a 10.5 μm pulse along the Cl–C–H bending direction (i.e. perpendicular to the C-H bond) gives a much higher percentage of the higher energy HCl^+ products (62.4%) at the expense of the lower energy Cl product. The average amount of vibrational energy absorbed from these two laser pulse sequences is very similar (Table 2), indicating that the difference in the branching ratio was not a result of differences in the amount of energy deposited into the vibrational modes by the laser pulses. This implies that a more complex mechanism may be involved in promoting the higher energy HCl^+ channel. One possibility is that the C–H stretching mode needs to be sufficiently energized before the C-H bending mode can drive the H atom toward Cl forming a H–Cl bond while the C–Cl bond is breaking. This concerted process requires less energy than C–H bond breaking followed by migration to the Cl. This suggests that the relative timing of the 3.5 μm and 10.5 μm pulses could matter. The data in Table 2 shows that this is indeed the case. When the 10.5 μm pulse is delayed by one quarter of the pulse duration, the yield of HCl^+ is increased to 72.7%, but when the 3.5 μm pulse is delayed by one quarter of the pulse duration, the yield of HCl^+ is decreased to 38.2%. This effect is considerably smaller when the delay between two pulses is extended to half of the pulse duration. When the 3.5 μm pulse is delayed, the vibrational energy gained from the laser in the HCl^+ channel is 20 kcal/mol lower than when the 10.5 μm pulse is delayed. This further supports the suggestion that the C-H bond must be energized first before bending can promote the formation of HCl^+.

Continuous wavelet transformation analysis

To obtain a better description of the laser induced dissociation of $ClCHO^+$, we need a method for examining the interaction of the laser pulse with various vibrational modes as a function of time. In particular, we would like to analyze the trajectories to obtain frequency domain information vs time to get some details about the energy in various vibrational modes as a function of time during and after the laser pulse. Windowed Fourier transformation (or Short-time Fourier transformation) is one approach. However, the window width needed to resolve the vibrational frequencies considered, ca. 350–4000 cm^{-1}, results in a time-frequency resolution that is too low. Wavelet transformation has the distinct advantage of having an adaptive time-frequency resolution, *i.e.* a higher time-domain resolution at higher frequencies (at the expense of frequency-domain resolution, constrained by uncertainty principle). We chose the continuous wavelet transformation (CWT) as opposed to the discrete wavelet transformation (DWT) used in signal processing, since we need a continuous function of time. The frequency range shown in Figure 4 (368–5897 cm^{-1}) was divided into 33 intervals distributed logarithmically. CWT was used to analyze each component of the square root mass weighted atomic velocities for each atom. The power spectrum for each component was summed to give the power spectrum for an individual trajectory as a function of time; the results for each trajectory in a specific reactive channel were averaged to get the average power spectrum for the ensemble of trajectories in that channel.

Table 2. Branching ratio and total vibrational energy absorption for various laser pulse sequences

wavelength and orientation			branching ratio (number of trajectories)[a]			Vibrational energy absorption (kcal/mol) [b]		
first pulse	second pulse	delay for 2nd pulse	H dissociation	Cl dissociation	HCl^+ dissociation	H dissociation	Cl dissociation	HCl^+ dissociation
7 μm (0.06 au) perpendicular to C–H bond		none	2.3% (2)	78.6% (66)	19.0% (16)	62.4	73.9 ± 61.9	106.3 ± 46.4
7 μm (0.03 au)	14 μm (0.03 au)	none	2.8% (4)	93.1% (135)	4.1% (6)	59.2	63.1 ± 44.6	93.4 ± 37.9
C–O stretch	C–Cl stretch							
3.5 μm(0.03 au)	10.5 μm(0.03 au)	none	1.1% (1)	36.6% (34)	62.4% (58)	51.8	74.1 ± 41.3	112.2 ± 30.4
C–H stretch	Cl–C–H bend							
3.5 μm (0.03 au)	10.5 μm (0.03 au)	¼ pulse width	1.8% (1)	25.5% (14)	72.7% (40)	116.4	63.7 ± 39.9	115.8 ±30.9
C–H stretch	Cl–C–H bend							
10.5 μm (0.03 au)	3.5 μm (0.03 au)	¼ pulse width	1.5% (1)	60.3% (41)	38.2% (26)	61.5	69.3 ± 34.9	95.1 ± 21.0
Cl–C–H bend	C–H stretch							
3.5 μm (0.03 au)	10.5 μm (0.03 au)	½ pulse width	3.4% (2)	55.9% (33)	40.7% (24)	116.2	64.7 ± 38.0	106.4 ± 26.9
C–H stretch	Cl–C–H bend							
10.5 μm (0.03 au)	3.5 μm (0.03 au)	½ pulse width	1.5% (1)	65.2% (43)	33.3% (22)	47.3	60.5 ± 36.2	92.9 ± 24.0
Cl–C–H bend	C–H stretch							

[a] Branching ratios for the three reactive channels.
[b] Values are average ± one standard deviation.

The results of the CWT analysis are shown in Figure 4. Four important peaks corresponding to vibrational or rotational modes in $ClCHO^+$ and its dissociation fragments can be easily identified by comparison with the calculated harmonic vibrational frequencies, namely C–H stretching in $ClCHO^+$ and HCO^+, C–O stretching in $ClCHO^+$, $ClCO^+$, HCO^+ and CO, C–H bending in $ClCHO^+$ and CHO^+, and HCl^+ rotation in the HCl^+ fragment. The changes in the intensities of the peaks is a result of the laser field driving specific vibrational modes and the flow of energy between modes. The changes in the positions of the peaks with time is the result of $ClCHO^+$ modes disappearing and fragment modes appearing as the molecule dissociates.

The six plots in Figure 4 correspond to three laser pulse sequences for the Cl dissociation channel and the HCl^+ dissociation channel. Too few trajectories produced H dissociation to be directly comparable with the other two dissociation channels. For Cl dissociation, $ClCHO^+ \rightarrow Cl + HCO^+$, the C-H stretching frequency increases a little (2983 $cm^{-1} \rightarrow$ 3229 cm^{-1}), the C=O stretch increases significantly (1507 $cm^{-1} \rightarrow$ 2270 cm^{-1}), the C-H bend decreases (1174 $cm^{-1} \rightarrow$ 865 cm^{-1}) and the C-Cl stretch (732 cm^{-1}) disappears. The 3.5 μm laser pulse drives the C-H stretch before dissociation but not afterwards. The pulses do not seem to activate the C-Cl stretching mode (perhaps because the C-Cl stretching frequency and polarization direction do not overlap sufficiently with the 10.5 μm pulse). The laser pulses activate the C=O stretching and C-H bending modes before dissociation. The increase in the C=O stretching frequency and decrease in the C-H bending frequency after dissociation can be seen in all three pulse sequences, but these changes are clearest in Figure 4(c) when the 3.5 μm pulse is delayed. Delaying the 3.5 μm pulse by a quarter of the pulse width increase the yield of Cl dissociation by nearly a factor of two. This suggests that this pulse sequence promotes Cl dissociation by increasing C-H bending rather than by increasing C-Cl stretching.

The plots for HCl^+ dissociation, $ClCHO^+ \rightarrow HCl^+ + CO$, are shown in Figure 4(d)-(f). Before dissociation, the laser pulses activate the C-H stretching mode early and C-H bending mode a little later. The C=O stretch is activated to a lesser extent. These effects are seen more clearly Figure 4(e) when the 3.5 μm pulse comes before the 10.5 μm pulse. After dissociation, the C-H stretching and bending modes disappear. The C=O stretching frequency and amplitude increases significantly, and a band for HCl^+ rotation appears. There may also be some HCl^+ stretching (2635 cm^{-1}), but this is uncertain because of the small amplitude and the low resolution in the frequency. The yield of HCl^+ is largest (72.7%) when the 3.5 μm pulse comes before the 10.5 μm pulse. This suggests that this pulse sequence promotes HCl^+ dissociation by first increasing C-H stretching and then C-H bending rather than by increasing C-Cl stretching. The significant amount of rotation seen in the plot is consistent with the hydrogen migrating to the chlorine during dissociation.

Conclusions

Our previous study showed that a single, very intense 7 μm linearly polarized laser pulse could dramatically increase the yield of

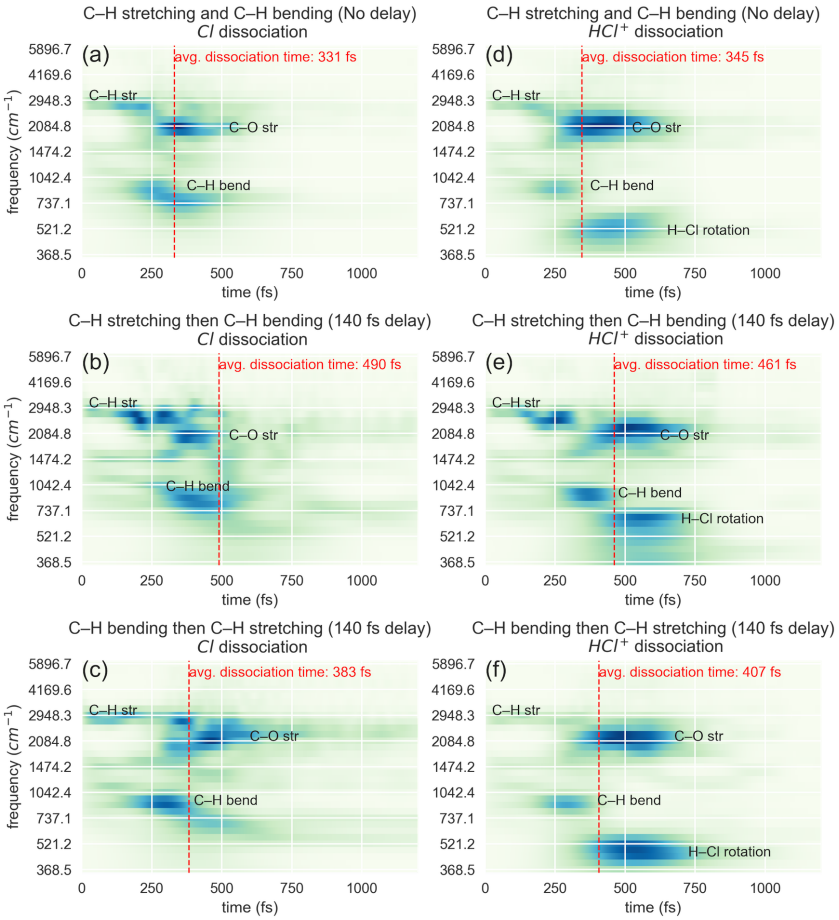

Figure 4. CWT analysis for Cl dissociation (panels (a), (b) and (c)), and HCl^+ dissociation (panels (d), (e), and (f)). Darker color indicates stronger signal. Vertical axis is in logarithm scale. Red vertical lines indicate average dissociation time. [Color figure can be viewed at wileyonlinelibrary.com]

the higher energy HCl^+ dissociation channel when the pulse was aligned perpendicular to the C-H bond.[9] In the present study, we explored the possibility of employing two different, moderate intensity mid-IR laser pulses to enhance the yield of higher energy reaction channels. Simultaneously promoting the C-H stretching mode (3.5 μm pulse along C-H bond) and the C-H bending mode (10.5 μm pulse perpendicular to C-H bond) gives a higher branching ratio for HCl^++CO dissociations than a comparable 7 μm pulse perpendicular to C-H bond. This effect depends strongly on the order in which the two pulses are applied. When the 10.5 μm pulse was delayed by one quarter of the pulse envelope, the branching ratio for HCl^++CO (73%) was a factor of three larger than the low energy channel (Cl + HCO^+, 25%). However, when the 3.5 μm pulse was delayed by one quarter of the pulse envelope, the branching ratio was reversed (HCl^++CO 38%; Cl + HCO^+, 60%). This suggests that the C-H bond must be energized first before bending can drive the hydrogen toward the chlorine to form HCl^+. Continuous wavelet transformation was used to follow the activation of vibrational and rotational modes by the laser pulses during the dissociation.

Acknowledgement

The authors would like to thank National Science Foundation for funding (NSF-CHE1464450) and the Wayne State University Grid for computer time.

Keywords: Strong field chemistry · mode selective chemistry · - Born-Oppenheimer molecular dynamics · aligned molecules · wavelet analysis

How to cite this article: X. Shi, H. B. Schlegel. *J. Comput. Chem.* **2019**, 40, 200–205. DOI: 10.1002/jcc.25576

[1] P. A. Schulz, A. S. Su, D. J. Krajnovich, H. S. Kwok, Y. R. Shen, Y. T. Lee, Annu Rev Phys Chem **1979**, 30, 379.
[2] F. F. Crim, Science **1990**, 249, 1387.
[3] D. J. Nesbitt, R. W. Field, J Phys Chem **1996**, 100, 12735.
[4] E. W.-G. Diau, J. L. Herek, Z. H. Kim, A. H. Zewail, Science **1998**, 279, 847.
[5] A. H. Zewail, J Phys Chem A **2000**, 104, 5660.
[6] R. J. Levis, G. M. Menkir, H. Rabitz, Science **2001**, 292, 709.
[7] L. Windhorn, J. S. Yeston, T. Witte, W. Fuß, M. Motzkus, D. Proch, K.-L. Kompa, C. B. Moore, J Chem Phys **2003**, 119, 641.
[8] T. Stensitzki, Y. Yang, V. Kozich, A. A. Ahmed, F. Kössl, O. Kühn, K. Heyne, Nat Chem **2018**, 10, 126.
[9] S. K. Lee, A. G. Suits, H. B. Schlegel, W. Li, J Phys Chem Lett **2012**, 3, 2541.
[10] S. K. Lee, H. B. Schlegel, W. Li, J Phys Chem A **2013**, 117, 11202.
[11] B. Thapa, H. B. Schlegel, J Phys Chem A **2014**, 118, 10067.
[12] B. Thapa, H. B. Schlegel, Chem Phys Lett **2014**, 610-611, 219.
[13] X. Shi, W. Li, H. B. Schlegel, J Chem Phys **2016**, 145, 084309.
[14] X. Shi, B. Thapa, W. Li, H. B. Schlegel, J Phys Chem A **2016**, 120, 1120.
[15] Y.-J. Tu, H. B. Schlegel, Submitted to Mol. Phys. **2018**, (accepted), (10.1080/00268976.2018.1506175)
[16] Y. Meyer, Wavelets and Operators, Cambridge University Press, Cambridge, **1992**.

[17] C. K. Chui, An Introduction to Wavelets, Academic Press, San Diego, **1992**.
[18] A. N. Akansu, R. A. Haddad, Multiresolution Signal Decomposition: Transforms, Subbands, Wavelets, Academic Press, San Diego, **1992**.
[19] Frisch, M. J.; Trucks, G. W.; Schlegel, H. B.; Scuseria, G. E.; Robb, M. A.; Cheeseman, J. R.; Scalmani, G.; Barone, V.; Mennucci, B.; Petersson, G. A.; Nakatsuji, H.; Caricato, M.; Li, X.; Hratchian, H. P.; Izmaylov, A. F.; Bloino, J.; Zheng, G.; Sonnenberg, J. L.; Hada, M.; Ehara, M.; Toyota, K.; Fukuda, R.; Hasegawa, J.; Ishida, M.; Nakajima, T.; Honda, Y.; Kitao, O.; Nakai, H.; Vreven, T.; Montgomery Jr., J. A.; Peralta, J. E.; Ogliaro, F.; Bearpark, M. J.; Heyd, J.; Brothers, E. N.; Kudin, K. N.; Staroverov, V. N.; Kobayashi, R.; Normand, J.; Raghavachari, K.; Rendell, A. P.; Burant, J. C.; Iyengar, S. S.; Tomasi, J.; Cossi, M.; Rega, N.; Millam, N. J.; Klene, M.; Knox, J. E.; Cross, J. B.; Bakken, V.; Adamo, C.; Jaramillo, J.; Gomperts, R.; Stratmann, R. E.; Yazyev, O.; Austin, A. J.; Cammi, R.; Pomelli, C.; Ochterski, J. W.; Martin, R. L.; Morokuma, K.; Zakrzewski, V. G.; Voth, G. A.; Salvador, P.; Dannenberg, J. J.; Dapprich, S.; Daniels, A. D.; Farkas, Ö.; Foresman, J. B.; Ortiz, J. V.; Cioslowski, J.; Fox, D. J., Gaussian Development Version, Gaussian, Inc.: Wallingford, CT, USA: **2015**, Rev. H.35.
[20] H. B. Schlegel, J Chem Theory Comput **2013**, 9, 3293.
[21] V. Bakken, J. M. Millam, H. B. Schlegel, J Chem Phys **1999**, 111, 8773.
[22] H. Wu, M. Rahman, J. Wang, U. Louderaj, W. L. Hase, Y. Zhuang, J Chem Phys **2010**, 133, 074101.
[23] D. L. Bunker, J Chem Phys **1973**, 59, 4621.
[24] O'Leary, A., *Continuous wavelet transforms in Python*, **2013**, (https://github.com/aaren/wavelets)

Received: 23 May 2018
Revised: 21 July 2018
Accepted: 25 July 2018
Published online on 14 October 2018